Published in final edited form as:
Nanomedicine (Lond). 2011 August ; 6(6): 975–994. doi:10.2217/nnm.11.27.

Macrophage endocytic trafficking of antiretroviral nanoparticles

Irena Kadiu[1,*], **Ari Nowacek**[1,*], **JoEllyn McMillan**[1], and **Howard E Gendelman**[1,†]
Department of Pharmacology & Experimental Neuroscience, University of Nebraska Medical Center, 985800 Nebraska Medical Center, Omaha, NE, 68198-5880 USA

Abstract

Aim—Nanoformulated antiretroviral therapy can improve drug compliance for people infected with HIV. Additional benefits would include specific drug deliveries to viral reservoirs and reduction in systemic toxicities.

Methods—In this article, we describe mechanisms of crystalline antiretroviral nanoparticle (NP) uptake, intracellular trafficking and release in human monocyte-derived macrophages.

Results—Following clathrin-dependent endocytosis NPs bypassed lysosomal degradation by sorting from early endosomes to recycling endosome pathways. Disruption of this pathway by siRNAs or brefeldin-A impaired particle release. Proteomic and biological analysis demonstrated that particle recycling was primarily Rab11 regulated. Particles were released intact and retained complete antiretroviral efficacy.

Conclusion—These results suggest possible pathways of subcellular transport of antiretroviral nanoformulations that preserve both particle integrity and antiretroviral activities demonstrating the potential utility of this approach for targeted drug delivery.

Keywords

antiretroviral therapy; drug delivery; endocytic trafficking; HIV; homogenization; monocyte-derived macrophages; nanoformulated antiretroviral drugs; Rab11; recycling endosomes

The need for simple antiretroviral therapeutic (ART) regimens for treating HIV-infected people are significant as the epidemic grows and broad access to drugs remain limited. This is particularly noteworthy for patients in resource-limited settings, with poor compliance, who have mal-absorption syndromes, and to combat common drug toxicities [1–5]. Although ART has drastically decreased the morbidity and mortality associated with advanced viral infection, ART effectiveness is hampered by its pharmacokinetic and biodistribution properties [6–9]. Owing to these factors it is difficult to maintain therapeutic drug levels and target drug delivery to infected tissues. Consequently, ART necessitates continuous and often complex dosing regimes that can result in systemic toxicities and are

†Author for correspondence: Tel.: +1 402 559 8910, Fax: +1 402 559 3744, hegendel@unmc.edu.
*Authors contributed equally

Ethical conduct of research
The authors state that they have obtained appropriate institutional review board approval or have followed the principles outlined in the Declaration of Helsinki for all human or animal experimental investigations. In addition, for investigations involving human subjects, informed consent has been obtained from the participants involved.

Financial & competing interests disclosure
This work was supported by NIH grants PO1 DA028555, P20 RR15635, 1 P01 NS043985-01, 2R37 NS36126, 5 P01 DA026146 and 5 P01 MH64570-03. The authors have no other relevant affiliations or financial involvement with any organization or entity with a financial interest in or financial conflict with the subject matter or materials discussed in the manuscript apart from those disclosed. No writing assistance was utilized in the production of this manuscript.

still limited in their access to viral sanctuaries [10–15]. An ideal delivery system, if developed, would increase ART stability and circulation time, improve biodistribution, and target infected cells and tissues. Crystalline antiretroviral nanoparticles (nanoART) were developed in our laboratories toward the goal of substantively increasing drug-dosing intervals, reducing drug concentrations for administration, facilitating drug access to viral sanctuaries, diminishing untoward side effects and improving drug availability to infected individuals. The latter targets patients who show poor compliance, have limited oral drug absorption or have few opportunities to obtain needed medicines.

Studies performed in our laboratory show that monocytes and monocyte-derived macrophages (MDMs) used for nanoART carriage possess superior stability, less toxicity and potent antiret-roviral efficacy compared with unformulated drugs [16–19]. Indeed, nanoART-laden MDMs are able to cross biological barriers in response to cytokine signaling, deliver drug(s) directly to infected tissues and drastically reduce viral replication [20]. Other animal studies have supported the *in vitro* results and demonstrated that clinically relevant amounts of drug are present within both serum and tissues for up to 3 months after a single administration [21,22]. These studies further support cell-mediated drug delivery. Nonetheless and despite such encouraging results, little is known regarding the subcellular distribution of the drug particles within macrophages or the consequences of its transport. To this end, we tracked the subcellular journey of nanoART from the point of initial uptake to final release. We observed that following rapid clathrin-dependent internalization, drug particles undergo sorting into a recycling pathway and as such bypass degradation. Drug was released intact from MDMs and had no reduction in antiretroviral efficacy. Interestingly, particle trafficking routes may parallel what has been observed for HIV endocytic sorting. Such parallels between HIV and nanoART subcellular endocytic locale likely provides additional benefit in restricting viral replication. Taken together, our findings support a role for macrophage-mediated drug delivery as a therapeutic option for a more efficient and simplified drug regimen for HIV-infected people.

Materials & methods

Antibodies & reagents

Goat antibody (Ab) to Rab11 and Rab7, along with human siRNA to Rab8, Rab11 and Rab14, were purchased from Santa Cruz Biotechnology (CA, USA). SilenceMag siRNA delivery reagent and magnetic plates were purchased from Oz Biosciences (Marseille, France). Rabbit Ab to lysosome-associated membrane protein 1 (LAMP1) was purchased from Novus Biologicals (CO, USA). Rabbit Abs to early endosome antigen 1 (EEA1), clathrin, Rab8 and Rab14 were purchased from Cell Signaling Technologies (MA, USA). pHrhodo-dextran conjugate for phagocytosis, rhodamine phalloi-din, phalloidin Alexa Fluor 488 and 647, transferrin (Tfn) conjugated to Alexa Fluor 594, anti-rabbit Alexa Fluor 488, 594, 647, anti-mouse Alexa Fluor 488, 594, 647, anti-goat Alexa Fluor 488, ProLong Gold antifading solution with 4′,6-diamidino-2-phenylindole (DAPI) were all purchased from Molecular Probes (OR, USA). Dynasore and indomethacin were purchased from Sigma-Aldrich (MO, USA).

RTV-NP manufacturing & characterization

Ritonavir nanoparticles (RTV-NPs) were prepared by high-pressure homogenization using an Avestin C-5 homogenizer (Avestin, Inc., ON, Canada) as described previously [19,23]. Surfactants used to coat the drug crystals included poloxamer 188 (P188; Spectrum Chemicals, CA, USA), 1,2-distearoyl-phosphatidyl ethanolamine-methyl-polyethyleneglycol 2000 ($mPEG_{2000}$-DSPE) and 1,2-dioleoyl-3-trimethylammonium-propane (DOTAP), purchased from Avanti Polar Lipids, Inc. (AL, USA). To coat the

nanosized drug crystals, each surfactant was made up of (weight/vol %) P188 (0.5%), $mPEG_{2000}$-DSPE (0.2%) and DOTAP (0.1%). The nanosuspen-sions were formulated at a slightly alkaline pH of 7.8 using either 10 mM sodium phosphate or 10 mM HEPES as a buffer. Tonicity was adjusted with glycerin (2.25%) or sucrose (9.25%). Free base drug was added to the surfactant solution to make a concentration of approximately 2% [weight to volume ratio (%)]. The solution was mixed for 10 min using an Ultra-Turrax T-18 (IKA® Works Inc. [NC, USA]) rotor-stator mixer to reduce particle size. The suspension was homogenized at 20,000 psi for approximately 30 passes or until desired particle size was achieved. Size was measured using a HORIBA LA 920 light scattering instrument (HORIBA Instruments Inc., CA, USA). For determination of polydispersity and zeta potential, 0.1 ml of the suspension was diluted into 9.9 ml of 10 mM HEPES, pH 7.4, and analyzed by dynamic light scattering using a Malvern Zetasizer Nano Series (Malvern Instruments Inc., MA, USA). At least four iterations for each reading were taken and the readings varied by less than 2%. After the desired size was achieved, samples were centrifuged and the resulting pellet resuspended in the surfactant solution containing 9.25% sucrose to adjust tonicity. Particle size and shape were characterized by scanning electron microscopy as described below. RTV-NPs were fluorescently labeled using the Vybrant 1,1′dioctadecyl-3,3,3′,3′-tetramethylindodicarbocyanine perchlorate (DiO) cell-labeling solution (Ex: 484 nm; Em: 501 nm) or 3,3′-dioctadecyloxacar-bocyanine perchlorate (DiD; Ex: 644 nm; Em: 665 nm; Invitrogen [CA, USA]). Particles were labeled by combining 1 ml of RTV-NP suspension with 5 μl of dye and mixing overnight. After centrifugation at 20,000 × g, the particles were washed with 5% human serum containing Dulbecco's modified Eagle medium (DMEM) until all excess dye was removed (at least five washes). Final drug content of the formulations were determined by high-performance liquid chromatography (HPLC; data not shown).

Human monocyte isolation & cultivation

Human monocytes were obtained by leukapheresis from HIV and hepatitis seronegative donors, and were purified by counter-current centrifugal elutriation following approval by the Institutional Review Board at the University of Nebraska Medical Center. Wright-stained cyto-spins were prepared and cell purity assayed by immunolabeling with anti-CD68 (clone KP-1). Monocytes were cultivated at a concentration of 1×10^6 cells/ml at 37°C in a humidified atmosphere (5% CO_2) in DMEM supplemented with 10% heat-inactivated pooled human serum, 1% glutamine, 50 μg/ml gentamicin, 10 μg/ml ciprofloxacin and 1000 U/ml recombinant human macrophage colony-stimulating factor (MCSF), a generous gift from Pfizer Inc. (MA, USA). To induce differentiation to macrophages, monocytes were cultured for 7 days in the presence of MCSF.

RTV-NP uptake & release

Monocyte-derived macrophages (2×10^6 per well) were cultured with RTV-NPs at 100 μM. Uptake of particles was assessed without medium change for 24 h with cell collection occurring at indicated times points. Adherent MDMs were collected by washing three times with 1 ml of phosphate-buffered saline (PBS), followed by scraping cells into 1 ml PBS. Samples were centrifuged at 950 × g for 10 min at 4°C and the supernatant removed. Cell pellets were sonicated in 200 μl of methanol and centrifuged at 10,000 × g for 10 min at 4°C. The methanol extracts were stored at −80°C until HPLC analysis was performed. After an initial 12-h exposure to RTV-NPs, drug release from MDMs with half media exchanges every other day was evaluated over a 2-week period. Media samples were saved along with replicate cells and stored at −80°C until HPLC analysis could be performed. Methanol-extracted cell suspensions were centrifuged at 21,800 × g at 4°C for 10 min. Media samples were thawed and deproteinated by the addition of methanol. The samples were centrifuged at 21,800 × g at 4°C for 10 min; supernatants were evaporated to dryness under vacuum and

resuspended in 75 μl of 100% methanol. Triplicate 20 μl samples of processed media or cells were assessed by HPLC using a YMC Pack Octyl C8 column (Waters Inc. [MA, USA]) with a C8 guard cartridge. Mobile phase consisting of 47% acetonitrile/53% 25mM KH_2PO_4, pH 4.15, was pumped at 0.4 ml/ min with UV/Vis detection at 212 nm. Cell and medium levels of RTV were determined by comparison of peak areas to those of a standard curve of free drug (0.025–100 μg/ml) made in methanol.

Immunocytochemistry & confocal microscopy

For immunofluorescence staining, cells were washed three times with PBS and fixed with 4% paraformaldehyde (PFA) at room temperature for 30 min. Cells were treated with blocking/permeabilizing solution (0.1% Triton, 5% bovine serum albumin [BSA] in PBS) and quenched with 50 mM NH_4Cl for 15 min. Cells were washed once with 0.1% Triton in PBS and sequentially incubated with primary and secondary Ab, at room temperature. For MDMs stained with multiple Abs, nonspecific cross binding of secondary Abs was tested prior to immunostaining. Use of secondary Abs originating or recognizing the same hosts was avoided. Slides were covered in ProLong Gold antifading reagent with DAPI and imaged using a 63× oil lens in a LSM 510 confocal microscope (Carl Zeiss Microimaging, Inc., NY, USA).

Imaging of recycling compartments

Monocyte-derived macrophages grown in poly-D-lysine-coated chamber slides were depleted of human serum by incubation with serum-free DMEM for 3 h. Cells were coincubated with 1 μM Alexa 594-Tfn and 100 μM DiO-labeled RTV-NPs for 4 h. Noninternalized particulates were removed by three sequential washes with PBS. Cells were fixed with 4% PFA and imaged using the 63× oil lens of a LSM 510 confocal microscope (Carl Zeiss Microimaging, Inc.).

Detection of acidified compartments

Monocyte-derived macrophages were exposed to pHrhodo conjugated to dextran beads and 100 μM DiO-labeled RTV-NPs at 37°C for 4 h. Noninternalized particulates were removed by washing three times in Hanks Balanced Salt Solution, pH 7.4, followed by fixation with 4% PFA and imaging. Fluorescence intensity of pHrhodo dye at different pH levels (3.0–8.5) was previously determined using a M5 Florescence Microplate Reader (Molecular Devices [CA, USA]).

Inhibition of RTV-NP uptake

Monocyte-derived macrophages were washed three times in PBS and incubated with serum-free medium for 30 min. Cells were then exposed to 100 μM dynasore, 100 μM indomethacin, and a combination of both for 30 min in serum-free medium or left untreated. Cells were washed once with serum-free media, and DiD-labeled 100 μM RTV-NPs reconstituted in serum-free medium was added together with fresh inhibitors to the MDMs for 3 h at 37°C. Cells were washed three times in PBS and mechanically detached using cell lifters. Cells were fixed in 4% PFA for 30 min and analyzed for RTV-NP uptake by flow cytometry. Data was acquired on a FACSCalibur flow cytometer using CellQuest Software (BD Biosciences, CA, USA). Replicate experiments were performed for HPLC analyses of drug content.

Electron microscopy

Samples were fixed by 3% glutaraldehyde in 0.1 M phosphate buffer (pH 7.4) and were further fixed in 1% osmium tetroxide in 0.1 M phosphate buffer (pH 7.4) for 1 h. Samples were dehydrated in a graduated ethanol series and embedded in Epon 812 (Electron

Microscopic Sciences [PA, USA]) for scanning electron microscopy. Thin sections (80 nm) were stained with uranyl acetate and lead citrate and observed under a transmission electron microscope (Hitachi H7500-I; Hitachi High Technologies America Inc. [IL, USA]).

Enrichment of endocytic compartments

For enrichment of RTV-NP-associated compartments, RTV-NPs were labeled with 0.01% Brilliant Blue R-250 dye (Thermo-Fisher Scientific, MA, USA) for 12 h at room temperature. Excess dye was removed by five washes in PBS and five subsequent centrifugations at 20,000 × g for 10 min. Then, 100 μM RTV-NPs were added to MDMs for 12 h at 37°C. Cells were washed three times in PBS, and RTV-NP uptake was visualized using the bright field settings on a Nikon Eclipse TE300 microscope (Nikon Instruments, Inc. [NY, USA]). Cells were detached in homogenization buffer (100 mM sucrose, 10 mM imidazole solution, pH 7.4) followed by 15 strokes on a Dounce homogenizer. Cellular debris and nuclei were removed by centrifugation at 500 × g for 10 min. Supernatant was mixed at equal ratios with 60% sucrose, 10 mM imidazole solution, pH 7.4, to adjust sucrose concentration to 30% followed by layering on a 60, 35, 20 and 10% sucrose gradient and centrifugation at 100,000 × g at 4°C for 1 h. The interface between 10–20 and 35–60% sucrose bands containing enriched endocytic compartments (blue) were collected. Pellets were collected by centrifugation at 100,000 × g at 4°C for 30 min, and sucrose was removed by washing three times in PBS. Pellets were then processed for proteomics analysis as described below.

Immune isolation of endocytic compartments was performed as described previously, with some modifications [24]. MDMs (400×10^6 cells) were treated with 100 μM RTV-NPs for 6 h. Cells were washed three times in PBS to remove extracellular RTV-NPs and then scraped in homogenization buffer (10 mM HEPES-KOH, pH 7.2, 250 mM sucrose, 1 mM EDTA and 1 mM $Mg(OAc)_2$). Cells were then disrupted by 15 strokes in a dounce homogenizer. Nuclei and unbroken cells were removed by centrifugation at 400 × g for 10 min at 4°C. Protein A/G paramagnetic beads (20 μl of slurry; Millipore) conjugated to EEA1, lysosome-associated LAMP1, and Rab11 antibodies (binding in 10% BSA in PBS for 12 h at 4°C) were incubated with the supernatants. Beads alone were also exposed to cell lysate to test for binding specificity. Following 24 h incubation at 4°C, $EEA1^+$, $LAMP1^+$ and $Rab11^+$ endocytic compartments were washed and collected on a magnetic separator (Invitrogen). The RTV-NP content of each compartment was determined by HPLC as described above.

Proteomic & mass spectrometry analyses

Endocytic compartments were solubilized in lysis buffer, pH 8.5 [30 mM TrisCl, 7 M urea, 2 M thiourea, 4% (w/v) 3-[(3-cholamidopro-pyl)dimethylammonio]-1-propanesulfonate, 20 mM dithiothreitol and 1X protease inhibitor cocktail (Sigma)] by pipetting. Proteins were precipitated using a 2D Clean up Kit and quantified by 2D Quant (GE Healthcare [WI, USA]) per the manufacturer's instructions. Samples were run on Bis-Tris 4–12% and 7% Tris-Glycine gels (Invitrogen) to separate low- and high-molecular-weight proteins. Electrophoresis was followed by fixation on 10% methanol, 7% acetic acid for 1 h and Coomassie staining at room temperature for 24 h. Bands were manually excised followed by in-gel tryptic digestion (10 ng/spot of trypsin [Promega, WI, USA]) for 16 h at 37°C. Peptide extraction and puri- ZipTips® (Millipore, MA, fication using μC_{18} USA) were performed on the Proprep Protein Digestion and Mass Spec Preparation Systems (Genomic Solutions, MI, USA).

Extracted peptides were fractionated on a column (New Objectives, microcapillary RP-C_{18} Inc. [MA, USA]) and sequenced using a liquid chromatography electrospray ionization tandem mass spectrometry system (ProteomeX System with LTQ-Orbitrap mass

spectrometer, Thermo-Fisher Scientific) in a nanospray con-figuration. The acquired spectra were searched against the NCBI.fasta protein database narrowed to a subset of human proteins using the SEQUEST search engine (BioWorks 3.1SR software from Thermo-Fisher Scientific). The TurboSEQUEST search parameters were set as follows: Threshold Dta generation at 10000, Precursor Mass Tolerance for the Dta Generation at 1.4, Dta Search, Peptide Tolerance at 1.5 and Fragment Ions Tolerance at 1.00. Charge state was set on "auto". Database nr.fasta was retrieved from ftp.ncbi.nih.gov and used to create 'in-house' an indexed human.fasta.idx (keywords: *Homo sapiens*, human, primate). Proteins with two or more unique peptide sequences ($p < 0.05$) were considered highly confident.

siRNA treatment & Western blotting

siRNA was combined with magnetic beads, and MDMs were transfected as indicated by the manufacture's instructions and then cultured for an additional 72 h in order to achieve maximal protein knockdown. Protein removal was con-firmed by Western blotting. Protein samples were quantified using the Pierce 660-nm Protein Assay and Pre-diluted Protein Assay BSA Standards to standardize the curve (Thermo Scientific [IL, USA]). From each protein sample, 10–15 μg was loaded and electrophoresed on a NuPAGE® Novex 4–12% Bis–Tris gel (Invitrogen); the gel was transferred to a polyvinylidene fluoride membrane (Bio-Rad Laboratories [CA, USA]). The membrane was blocked with 5% powdered milk/5% BSA in PBS-T and then probed with primary Ab followed by secondary Ab. Protein bands were distinguished using SuperSignal® West Pico Chemiluminescent substrate (Pierce [IL, USA]). siRNA-transfected MDMs were then treated with 100 μM RTV-NPs followed by harvesting of cells and replicate media samples and drug analysis by HPLC.

Macrophage RTV-NP release & dissociation to free drug

Cell culture medium was collected from RTV-NP-loaded MDMs 18 h after drug loading to cells. Intact RTV-NPs were separated from dissolved drug by centrifugation at 100,000 × g on a Beckman TL-100 Ultracentrifuge (Brea [CA, USA]) for 1 h at 4°C. The resulting supernatants and NP pellets were processed for drug quantitation by HPLC.

Antiretroviral activities of RTV

Monocyte-derived macrophages were treated with equal amounts of RTV either in the non-formulated state dissolved in ethanol (0.01% final concentration), native RTV-NPs or released RTV-NPs for 12 h and then washed. Drug-treated MDMs were infected at a multiplicity of infection of with HIV_{ADA} 0.01 infectious viral particles/cell [25] on day 1 after RTV-NP treatment. Following viral infection, cells were cultured for 10 days with half media exchanges every other day. Media samples were collected 10 days after infection for measurement of progeny virion production as assayed by reverse transcriptase (RT) activity [26]. Parallel analyses for expression of HIV p24 antigen in infected cells were performed by immunostaining using p24 mouse mono-clonal Ab (Dako [CA, USA]) on the same day as media sampling.

RT assay

In a 96-well plate, media samples (10 μl) were mixed with 10 μl of a solution containing 100 mM Tris-HCl (pH 7.9), 300 mM KCl, 10 mM dithiothreitol, 0.1% nonyl phenoxyl-polyethoxylethanol-40 (NP-40) and water. The reaction mixture was incubated at 37°C for 15 min and 25 μl of a solution containing 50 mM Tris-HCl (pH 7.9), 150 mM KCl, 5 mM dithiothreitol, 15 mM $MgCl_2$, 0.05% NP-40, 10 μg/ml poly(A), 0.250 U/ml oligo and 10 μCi/ml tritiated thymidine $d(T)_{12–18}$ triphosphate was added to each well; plates were incubated at 37°C for 18 h. Following incubation, 50 μl of cold 10% TCA was added to each well; the wells were harvested onto glass fiber filters, and the filters were assessed for

tritiated thymidine triphosphate incorporation by β-scintillation spectroscopy using a TopCount NXT (PerkinElmer Inc. [MA, USA]) [26].

Immunohistochemistry & quantitation of HIV-1 p24 staining

A total of 10 days after HIV-1 infection, cells were fixed with 4% phosphate-buffered PFA for 15 min at room temperature. Fixed cells were blocked with 10% BSA in PBS containing 1% Triton X-100 for 30 min at room temperature and incubated with mouse monoclonal antibodies to HIV-1 p24 (1:100, Dako) for 3 h at room temperature. Binding of p24 Ab was detected using a Dako EnVision$^+$ System-HRP labeled polymer anti-mouse secondary Ab and diaminobenzidine staining. Cell nuclei were counterstained with hematoxylin for 60 s. Images were taken using a Nikon TE300 microscope with a 40× objective. Quantitation of immunostaining was performed by densitometry using Image-Pro Plus, v. 4.0 (Media Cybernetics Inc. [MD, USA]). Expression of p24 was quantified by determining the positive area (index) as a percentage of the total image area per microscopy field.

Statistical analyses

Quantitation of immunostaining was performed with ImageJ software, utilizing JACoP plugins [101] to calculate Pearson's colocalization coefficients. Comparison was performed on three to five sets of images acquired with the same optical settings. Graphs and statistical analyses were generated using Excel and Prism software (GraphPad Software, Inc. [CA, USA]). Significant differences in drug levels in uptake and release studies were determined by two-way ANOVA followed by Bonferroni's Multiple Comparison Test. Significant differences in RT activity, p24 density and drug content in siRNA experiments were determined by one-way ANOVA followed by Dunnett's Multiple Comparison Test. Two-tailed Student's *t*-tests were used for all other data; and unless otherwise noted, the error bars are shown as ± standard error of the mean (SEM). Results were considered significant at $p < 0.05$.

Results

Characterization & *in vitro* pharmacokinetics of RTV-NPs

Ritonavir NPs were a representative formulation of nanoART and used as such for assays of cell particle localization and release. The RTV-NP consisted of drug crystals of free-base RTV coated with a thin layer of phospholipid surfactants of $mPEG_{2000}$-DSPE, P188 and DOTAP. Physical properties (size, shape and zeta potential) of the particles are shown in Figure 1A. P188 and $mPEG_{2000}$-DSPE increased particle stability, while the DOTAP coating enabled a positive surface charge. The polydispersity index was 0.196, indicating that while the majority of RTV-NPs were the calculated average measured size, the overall particle population was heterogeneous. Of note, p188 alone, P188/$mPEG_{2000}$-DSPE or P188/$mPEG_{2000}$-DSPE-DOTAP do not affect RTV-NP cell uptake [19,23]. Scanning electron microscopy revealed smooth rod-like morphologies for the RTV-NPs and confirmed size measurements and distribution (Figure 1B).

We assessed the cell-based pharmacokinetics of RTV-NP MDM uptake and release. Cells were exposed to 100 μM RTV-NPs in DMEM and drug uptake was assessed by HPLC. This drug concentration was chosen based upon previous observations that demonstrated it had limited cellular toxicity and potent antiretroviral efficacy when assayed by (3-(4,5-dimethylthiazol-2-yl)-2,5-diphenyltetr azolium bromide, a yellow tetrazole) assay and RT activity, respectively [18,19]. RTV-NP internalization in MDMs was observed at 30 min and peaked at 4 h (Figure 1C). Internalized particles were detected in MDMs for up to 15 days (Figure 1D).

To assay the mechanism of RTV-NP entry into macrophages, chemical blockers were used to inhibit clathrin- and caveolae-mediated cell entry. After pretreatment with 100 μM dynasore (prevents clathrin-coated pit formation through inhibition of dynamin) or indomethacin (caveolae inhibitor) for 1 h, MDMs were exposed to fluorescent RTV-NPs. Flow cytometry and HPLC analyses demonstrated that RTV-NP internalization occurs through clathrin-coated pits (Figure 1e & 1F).

Proteomic analysis identifies RTV-NP-containing endocytic compartments

Imaging of RTV-NP-laden MDMs by transmission electron microscopy confirmed uptake of intact particles into distinct cytoplasmic vesicles (Figure 2A). We then investigated the subcellular distribution of RTV-NPs within MDMs. RTV-NPs were labeled with Brilliant Blue R-250 dye and added to MDMs for 12 h. MDMs were mechanically disrupted and RTV-NPs containing endo-cytic compartments (blue) were collected as blue bands on a sucrose gradient (Figure 2B). Mass spectrometry analyses of the fractions identified 38 proteins associated with distinct endosomal populations (TABle 1). Based on their postulated subcellular localization, the proteins were classified into clathrin-coated pits, early endosomes (EE), recycling endosomes (RE), multivesicular bodies, late endosomes (LE), and lysosomes (L). Proteins were distributed predominantly in early and recycling endocytic cell compartments (EE [24%] and RE [22%]) (Figure 2C). These data support the role of recycling compartments in intracelluar sorting of RTV-NPs.

Confocal microscopy for RTV-NP subcellular distribution

To further substantiate proteomic findings, we performed confocal microscopy to visualize and quantitate the subcellular distribution of RTV-NPs with early (EEA1), recycling (Rab8, 11, 14) and degrading endocytic compartments (late degrading endosomes [Rab7]) and L (LAMP1). MDMs were treated with RTV-NPs fluorescently labeled with either DiD or DiO for 12 h and then immunostained for the endocytic compartments identified by proteomic analysis (Figure 3). Confocal imaging showed NP distribution in a punctate pattern throughout the cytoplasm and perinuclear region colocalizing predominantly with EE and RE (Figure 3A–H). Quantitation of fluorophore overlap using Pearson's co-localization tests showed significant accumulation ($p < 0.001$) of RTV-NPs with $EEA1^+$ (9.5 ± 0.4% [mean ± SEM]; n = 41) early endosomes and $Rab8^+$ (12.8 ± 0.2%; n = 56), $Rab11^+$ (31.0 ± 0.6%; n = 33) and $Rab14^+$ (22.8 ± 0.5%; n = 189) RE compared with degrading compartments such as Rab7 LE (4.1 ± 0.4%; n=47) and L (5.0 ± 0.9%; n = 28; Figure 3g). These data support the notion that the particles undergo endocytic recycling rather than degradation in human MDMs.

Disruption of endocytic recycling with siRNA & brefeldin A blocks RTV-NP release

To confirm the recycling pathway for RTV-NP trafficking, we suppressed Rab8, 11 and 14 by siRNA. MDMs exposed to siRNA and DiD-labeled RTV-NPs were analyzed by confocal microscopy for cellular distribution and HPLC for drug retention (cell lysates) and release (culture medium). Western blots using untreated MDMs and those exposed to either scrambled or targeted siRNA confirmed Rab protein silencing (Figure 4C). Confocal microscopy revealed that in siRNA-treated MDMs the distribution of RTV-NPs was considerably altered compared with untreated and scramble-treated MDMs (Figure 3 & 4A). Treated cells displayed a diminished codistribution of Rab8, 11 and 14 with RTV-NPs, loss of cytoplasmic punctate distribution and aggregation of the particles adjacent to the nucleus (Figure 4A). HPLC analyses indicated that cells treated with Rab11 and Rab14 siRNA retained more drug (Figure 4D) and released less drug (Figure 4e) into the media than untreated, siRNA scramble- and Rab8 siRNA-treated MDMs. Treatment with brefel-din A (BFA; a disruptor of recycling and secretory activities) yielded similar results, resulting in aggregation of RTV-NPs in the perinuclear region (Figure 4B). HPLC analyses showed that

MDMs treated with BFA retained more drug and released less drug than untreated and siRNA scramble-treated cells (Figure 4D & 4e). Consequently, considerably fewer RTV-NPs were detected in the culture media of the BFA-treated cells. Together these data demonstrate endocytic recycling routes in both intracellular trafficking and release of RTV-NPs.

Intact RTV-NP traffic between endocytic compartments

Minimal distribution of RTV-NPs with late degrading endosomes and L led us to question whether indeed the drug bypassed degradation pathways. Since only the surfactants (not the drug crystals) were fluorescently labeled with the lipophillic dyes DiD and DiO we investigated whether the particle was trafficked intact. Cells exposed to RTV-NPs were mechanically disrupted and the EE, RE and L were immuno-isolated using protein A/G paramagnetic beads conjugated to EEA1, Rab11 and LAMP1 (Figure 5A). Endocytic compartments bound to beads were collected by magnetic separation, digitally imaged and then analyzed by HPLC for drug content (Figure 5A). Interestingly, a thin layer of drug (white) covering the bead pellet (brown) was readily visible in the immuno-isolated Rab11 endosomes but not in other compartments (Figure 5B). Consistent with co-localization confocal tests, HPLC analysis confirmed the presence of drugs in Rab11 endosomes and, more importantly, at significantly greater amounts compared with EEA1- or LAMP1-associated vesicles (Figure 5C). These results indicate that the polymer coat and the drug crystal parts of RTV-NPs indeed undergo the same sorting (recycling) routes.

To determine whether the RTV-NPs are preserved during endocytic trafficking and released intact, we imaged RTV-NPs collected from culture fluids 24 h post-uptake in addition to measuring drug content. To avoid collection of original RTV-NPs, MDMs were exposed to DiD-labeled RTV-NPs for 12 h, thoroughly washed (five times in 1 ml of PBS), imaged with fluorescent microscopy to confirm the presence of only intracellular particles, and then allowed to release drug for 24 h post-uptake (data not shown). Scanning electron microscopy images show that released RTV-NPs are intact (Figure 6B) and display the same size and shape as the original particles (Figure 6A). However, the released particles displayed ragged edges and were released as aggregates (Figure 6B) as opposed to native particles that had smooth edges and were all individually distinct (Figure 6A). Since released RTV-NPs were identified in cell culture fluids, we determined the relative amount of drug that was present in particulate form compared with dissolved free drug. Particulate RTV was separated from soluble RTV by ultracentrifugation and quantitated by HPLC. As shown in Figure 6C, of the total amount of RTV, 32% was dissolved in culture medium, while 68% was present as intact NPs. These data indicate that the majority of drug is released from cells in particulate form.

Minimal distribution with acidic (degrading) compartments, as labeled by dextran-conjugated pH-sensitive dye (fluoresces bright red at pH <5.5), suggests that the mild pH environment of RE may preserve the integrity of RTV-NPs (Figure 3g). Additionally, considerable overlap of RTV-NPs with Tfn^{+} compartments suggests that fast recycling to the plasma membrane may also contribute to the preservation of intact particles (Figure 3e). These results indicate that RTV-NP physical properties and morphology are not affected during trafficking within the macrophage.

RTV-NPs maintain antiretroviral activities after cell release

To test whether antiretroviral activities were maintained after particle release, MDMs were exposed to equal concentrations of native RTV-NPs, released RTV-NPs and free drug followed by a challenge with HIV infection. Antiretroviral effects were measured by HIV p24 expression and RT activity. Pretreatment with free RTV provided no protection against

infection, while both native RTV-NPs and released RTV-NPs were equally able to significantly ($p < 0.01$) suppress HIV replication (p24 staining) and formation of multinucleated giant cells (Figure 6D & 6F). Reverse transcriptase activity was significantly suppressed in MDMs exposed to original and released RTV-NPs compared with untreated cells and those exposed to free drug (Figure 6e). These findings demonstrate that endocytic sorting does not affect antiretroviral efficacy of RTV-NPs and suggests a high potential of the macrophage as an efficient drug-laden particle delivery vehicle.

Discussion

Reformulating ART drugs into nanocrystals for transport by mononuclear phagocytes (MPs; monocytes and tissue macrophages) can improve clinical drug efficacy. Indeed, harnessing MPs as vehicles for drug delivery to HIV sanctuaries protected by biological barriers can serve both to simplify drug regimens and enhance their therapeutic index. ART medications are insoluble in water and thus can form stable crystals in aqueous solutions. Owing to their phagocytic and migratory functions MPs can readily ingest foreign material and cross into areas of microbial infection and inflammation. If loaded with drug NPs, these cells could potentially deliver drug(s) to sites that would otherwise be inaccessible due to the presence of either physical or biochemical barriers. MPs are ideal candidates for transporting nanoART since the cells are HIV targets and can act both as viral reservoirs and transporters [27–29].

In recent years, several important strides towards achieving clinical use for cell-based ART nanocarriage have been realized. First, formulations similar to those examined in this report have been developed for cancer chemotherapy and for a range of microbial infections. For the latter, liposomal amphotericin B (Ambisome®) is an example of a nanoformulation that enhances cure rates and reduces side effects for a variety of fungal diseases and as a result is now commonly used in the clinic [30–32]. Second, proof of concept was realized recently for the manufacture, cell uptake and release, and sustained plasma drug levels in human cells and in rodent models of human disease [33,34]. Third, integrations of research efforts between physical chemistry, cell biology and virology to obtain and test slow-release forms of antiretroviral agents are expedited by bioimaging and pharmaceutical testing [35–38]. Fourth, the notion that MP migratory function can be harnessed for therapeutic benefit makes practical sense as these same cells are viral targets and carriers, show robust phagocytic capabilities and readily migrate to areas of sustained viral growth and inflammation [27–29]. To this end, we investigated RTV-NP entry, intracellular trafficking and release. Indeed, the interactions between nanoART and macrophages is critical if therapeutic translation is to be achieved [39]. Interestingly, the majority of RTV-NPs were contained within compartments that provide a protected environment and allows for the particles to be released intact with retained antiretroviral activities. Importantly, RTV-NP endocytic compartments mirror those used in the HIV lifecycle. These results strongly support that cell-mediated delivery of active drug could be effective.

Through our prior works we have been able to achieve integration between formulation synthesis; *in vitro* testing for drug NP uptake, release, and cytotoxicity; and *in vivo* testing for pharmacokinetics [Gendelman H *et al*., Unpublished Data] [19,23]. Based on the limited cytotoxicities [40], we posit that sustained high levels of antiretroviral drug levels in virus-targeted tissues (including the lymphoid system and CNS) can be realized as observed in adoptive cell transfers [16,20]. However, to be used in the clinic, nanoART synthesis will have to be optimized, and this will require thoughtful integration in a cross-disciplinary manner. To address this, robust and scalable procedures for preparing nanoART formulations with optimal size, surface coating and colloidal stability need to be achieved in order to maximize uptake by circulating monocytes and delivery to sites of active viral

growth. Techniques such as precipitation, homogenization and wet milling could be used to prepare nanoART with adequate physical and chemical stability for sufficient drug loading, appropriate osmolarity, viscosity and sterility [41–43]. The size, shape and charge of the particles used in this study are starting points for such efforts.

Ritonavir NPs were used to model nanoART for descriptions of macrophage uptake and intracellular distribution of drug formulation. A thorough analysis of nanoART uptake, retention, release and cytotoxicity were shown previously [23,40]. For these works the cellular uptake and retention of nanoART were shown to be closely dependent on particle shape and surfactant, together with the chemical nature of the drug. While we offer unique insights into how macrophages process nanoART we caution that differences among the particles will probably be observed based on the physicochemical properties of the formulations. Using this model system, however, we demonstrate that the NPs primarily enter macrophages through a clathrin-mediated pathway [44]. The subcellular distribution of the NPs were seen in recycling endosomal compartments. Indeed, co-localization immunocytochemical studies demonstrated that there were significantly more RTV-NPs in RE, particularly within $Rab11^+$ vesicles, than in other compartments. The subcellular distribution pattern of RTV-NPs was concentrated in the perinuclear region, further supporting their localization to RE [45–48]. Although RTV-NP presence was also observed in LE and L due to limited particle overlap with acidic vesicles, it is likely that the particles contained within LE and L are not being degraded but redirected to recycling compartments. For example, Rab9, which we identified by proteomic analysis, is involved with the retrograde transport of LE that eventually fuse with the trans-Golgi network and are packaged into RE [49,50]. These results suggested that RTV-NPs avoided intra-cellular degradation and were primarily being stored within recycling compartments for eventual release at the cell surface. Functional studies demonstrated that the removal of proteins involved with the trafficking of RE inhibited drug release from RTV-NP-containing cells. In particular, Rab11, a marker for intracellular recycling [51–57], appeared to facilitate both particle trafficking and release. There are two main types of endosomal recycling: slow and fast. Rab11 along with Rab9, both of which were identified during proteomic analyses, have been recognized as proteins that participate in slow recycling [50,58–61]. In addition, Rab11 has been shown to play a role in exocytosis in that it can control the passage of material from the Golgi through endosomes and finally to the cell surface, known as slow recycling, as opposed to Rab8 and 14, which direct transit from the Golgi directly to the cell surface, known as fast recycling [62,63]. This could explain the differences we saw in the functional consequences of removal of the Rab proteins. In all cases, removal of the recycling Rab proteins caused the RTV-NPs to redistribute very densely near the nucleus, suggesting that all of these proteins are involved with particle trafficking. However, removal of Rab8 did not inhibit drug release and removal of Rab14 only slightly reduced it. On the other hand, removal of Rab11 had a very significant inhibitory effect, suggesting that while some particles may be released quickly, the primary mechanism probably involves slow recycling to the plasma membrane via $Rab11^+$ vesicles. It is worth noting that Rab11 has been implicated in the rapid recycling of Tfn [64], and we did observe an appreciable amount of particle co-localization with Tfn. It is probable that rapid recycling of RTV-NPs does occur since removal of Rab11 did not totally inhibit drug release; however, since RTV-NPs persist in MDMs for over 2 weeks, it is more likely that the majority of particles are indeed slowly recycled. A proposed pathway for intracellular trafficking of RTV-NPs from uptake to release is shown in Figure 7. Finally, Rab11 is known to recruit both actin- and microtubule-based motor protein complexes that transport vesicles along cytoskeletal filaments [65]. Many of these proteins were also identified during our proteomic analyses, suggesting that some of what we initially considered to be nonspecific labeling was actually correctly identifying the motor complexes and structural components involved with RTV-NP trafficking within $RAB11^+$ endosomes.

Taken together, these data uncover a pathway in which RTV-NPs avoid intracellular degradation and are recycled to the plasma membrane. First, we demonstrated this by visually identifying intact RTV-NPs that had been released from particle-laden MDMs. We further demonstrated that these released particles retained full antiretroviral activity. In this regard, MDMs uptake, retain, transport and release intact RTV-NPs that inhibit HIV replication, suggesting that macrophages can act as true 'Trojan horses' for nanoART, delivering active drug(s) to sites of viral infection. Second, it appears that RTV-NPs can inhibit viral replication via an intracellular mechanism since a small amount of RTV-NPs was able to completely suppress viral replication, while an equivalent amount of free drug had no effect. This facet of NP–macrophage interactions supports the idea that RTV-NPs, like HIV, enter macrophages through clathrin-coated pits [66]. In addition, a significant component of the virus' lifecycle occurs within RE [67,68]. Together, these findings imply that RTV-NPs could not only enter the cell along with HIV but could also have identical subcellular destinations, thus enabling drug targeting to specific subcellular compartments. This provides a cogent rationale for why nanoART, in the broader sense, could have potent antiretroviral effects even at very low intracellular concentrations [16–20,23]. Direct inhibition of HIV replication at the subcellular level would subsequently increase the therapeutic index of ART, thereby decreasing the amount of drug needed to inhibit viral replication.

Conclusion

The subcellular locale of the RTV-NPs and their slow release underlie long-term antiretroviral efficacy. Importantly, our results explain why nanoART is stable within macrophages for prolonged time periods. In addition, the data demonstrates that macrophages can act as drug transporters and, importantly, neither degrade nor modify drug-laden particles in transit. As such, biologically active drug(s) would be delivered unaltered to its intended target sites. Understanding the interactions between nano-formulated antiretroviral drugs and the virus lifecycle in its target cells is required for the complete development of nanoART for clinical use. The current detailed cell biologic and proteomic study of the uptake, subcellular distribution, retention and release of nanoformulated antiretroviral drug is an important first step toward realizing this goal.

Future perspective

The precise mechanisms of uptake and release of nanoART have now been determined. This addresses questions of particle trafficking within the cell compartments and resolves the query of how nanoART is maintained inside macrophages and secreted slowly over defined time periods. It is critical to now assay which subcellular compartments that the viral lifecycle utilizes are also components of nanoART endocytic trafficking. In this way, improved subcellular delivery of antiretroviral medicines may be realized. The linkages between *in vitro* observations and *in vivo* pharmacokinetics, biodistribution and antiretroviral properties need to be resolved. Specific studies are now being designed to compare antiretroviral efficacy of nanoART in humanized mouse models of HIV infection. This will shortly facilitate the realization of nanoART as a useful delivery system for HIV-1-infected people with limited access to drugs, with drug compliance issues, and for definitive needs secondary to impaired absorption and bioavailability.

Acknowledgments

The authors thank Robin Taylor for critical reading of the manuscript and outstanding graphic and literary support. The authors also thank Han Chen of the University of Nebraska-Lincoln electron microscopy core facility for supplying the scanning and transmission electron microscopy images. The authors would also like to thank Janice

Taylor and James Talaska of the UNMC Confocal Laser Scanning Microscope Core Facility for assisting with the acquisition of the confocal microscopy images.

Bibliography

Papers of special note have been highlighted as:

▪ of interest

▪ of considerable interest

1. Altice FL, Kamarulzaman A, Soriano VV, Schechter M, Friedland GH. Treatment of medical, psychiatric, and substance-use comorbidities in people infected with HIV who use drugs. Lancet. 2010; 376(9738):367–387. [PubMed: 20650518]
2. Beyrer C, Malinowska-Sempruch K, Kamarulzaman A, Kazatchkine M, Sidibe M, Strathdee SA. Time to act: a call for comprehensive responses to HIV in people who use drugs. Lancet. 2010; 376(9740):551–563. [PubMed: 20650515]
3. Chulamokha L, DeSimone JA, Pomerantz RJ. Antiretroviral therapy in the developing world. J Neurovirol. 2005; 11(Suppl 1):76–80. [PubMed: 15960241]
4. De Cock KM, De Lay P. HIV/AIDS estimates and the quest for universal access. Lancet. 2008; 371(9630):2068–2070. [PubMed: 18571714]
5. Wolfe D, Carrieri MP, Shepard D. Treatment and care for injecting drug users with HIV infection: a review of barriers and ways forward. Lancet. 2010; 376(9738):355–366. [PubMed: 20650513]
6. Broder S. The development of antiretroviral therapy and its impact on the HIV-1/AIDS pandemic. Antiviral Res. 2010; 85(1):1–18. [PubMed: 20018391]
7. Este JA, Cihlar T. Current status and challenges of antiretroviral research and therapy. Antiviral Res. 2010; 85(1):25–33. [PubMed: 20018390]
8. Moreno S, Lopez Aldeguer J, Arribas JR, et al. The future of antiretroviral therapy: challenges and needs. J Antimicrob Chemother. 2010; 65(5):827–835. [PubMed: 20228080]
9. Taiwo B, Hicks C, Eron J. Unmet therapeutic needs in the new era of combination antiretroviral therapy for HIV-1. J Antimicrob Chemother. 2010; 65(6):1100–1107. [PubMed: 20348088]
10. Anuurad E, Semrad A, Berglund L. Human immunodeficiency virus and highly active antiretroviral therapy-associated metabolic disorders and risk factors for cardiovascular disease. Metab Syndr Relat Disord. 2009; 7(5):401–410. [PubMed: 19355810]
11. Barbaro G. Visceral fat as target of highly active antiretroviral therapy-associated metabolic syndrome. Curr Pharm Des. 2007; 13(21):2208–2213. [PubMed: 17627554]
12. Kraft-Terry SD, Stothert AR, Buch S, Gendelman HE. HIV-1 neuroimmunity in the era of antiretroviral therapy. Neurobiol Dis. 2010; 37(3):542–548. [PubMed: 20044002]
13. Kramer AS, Lazzarotto AR, Sprinz E, Manfroi WC. Metabolic abnormalities, antiretroviral therapy and cardiovascular disease in elderly patients with HIV. Arq Bras Cardiol. 2009; 93(5):561–568. [PubMed: 20084320]
14. Rao KS, Ghorpade A, Labhasetwar V. Targeting anti-HIV drugs to the CNS. Expert Opin Drug Deliv. 2009; 6(8):771–784. [PubMed: 19566446]
15. Varatharajan L, Thomas SA. The transport of anti-HIV drugs across blood–CNS interfaces: summary of current knowledge and recommendations for further research. Antiviral Res. 2009; 82(2):A99–A109. [PubMed: 19176219]
16. Dou H, Destache CJ, Morehead JR, et al. Development of a macrophage-based nanoparticle platform for antiretroviral drug delivery. Blood. 2006; 108(8):2827–2835. [PubMed: 16809617]
17. Dou H, Morehead J, Destache CJ, et al. Laboratory investigations for the morphologic, pharmacokinetic, and anti-retroviral properties of indinavir nanoparticles in human monocyte-derived macrophages. Virology. 2007; 358(1):148–158. [PubMed: 16997345]
18. Nowacek AS, McMillan J, Miller R, Anderson A, Rabinow B, Gendelman HE. Nanoformulated antiretroviral drug combinations extend drug release and antiretroviral responses in HIV-1-infected macrophages: implications for neuroAIDS therapeutics. J Neuroimmune Pharmacol. 2010

19▪. Nowacek AS, Miller RL, McMillan J, et al. NanoART synthesis, characterization, uptake, release and toxicology for human monocyte-macrophage drug delivery. Nanomed (Lond). 2009; 4(8): 903–917. *In vitro* analysis demonstrated that nanoART are rapidly taken up and then slowly released by monocyte-derived macrophages. In addition, nanoART were shown to be highly efficacious against HIV replication.

20▪▪. Dou H, Grotepas CB, McMillan JM, et al. Macrophage delivery of nanoformulated antiretroviral drug to the brain in a murine model of neuroAIDS. J Immunol. 2009; 183(1):661–669. Demonstrated that macrophages loaded with nanoART could cross the blood–brain barrier, deliver drug to the brain and inhibit HIV replication in a mouse model of HIV encephalitis. [PubMed: 19535632]

21. Baert L, van't Klooster G, Dries W, et al. Development of a long-acting injectable formulation with nanoparticles of rilpivirine (TMC278) for HIV treatment. Eur J Pharm Biopharm. 2009; 72(3):502–508. [PubMed: 19328850]

22▪▪. Van't Klooster G, Hoeben E, Borghys H, et al. Pharmacokinetics and disposition of rilpivirine (tmc278) nanosuspension as a long-acting injectable antiretroviral formulation. Antimicrob Agents Chemother. 2010; 54(5):2042–2050. *In vivo* administration of crystalline ART nanoparticles allowed for sustained drug levels for up to 6 months. Observations suggested that nanoparticles were taken up by macrophages upon administration. [PubMed: 20160045]

23. Nowacek A, Balkundi S, McMillan J, et al. Analyses of nanoformulated antiretroviral drug charge, size, shape and content for uptake, drug release and antiviral activities in human monocyte-derived macrophages. J Control Release. Epub ahead of print. 10.1016/j.jconrel.2010.11.019

24. Basyuk E, Galli T, Mougel M, Blanchard JM, Sitbon M, Bertrand E. Retroviral genomic RNAs are transported to the plasma membrane by endosomal vesicles. Dev Cell. 2003; 5(1):161–174. [PubMed: 12852860]

25. Gendelman HE, Orenstein JM, Martin MA, et al. Efficient isolation and propagation of human immunodeficiency virus on recombinant colony-stimulating factor 1-treated monocytes. J Exp Med. 1988; 167(4):1428–1441. [PubMed: 3258626]

26. Kalter DC, Greenhouse JJ, Orenstein JM, Schnittman SM, Gendelman HE, Meltzer MS. Epidermal Langerhans cells are not principal reservoirs of virus in HIV disease. J Immunol. 1991; 146(10): 3396–3404. [PubMed: 2026871]

27. Meltzer MS, Gendelman HE. Mononuclear phagocytes as targets, tissue reservoirs, and immunoregulatory cells in human immunodeficiency virus disease. Curr Top Microbiol Immunol. 1992; 181:239–263. [PubMed: 1424782]

28. Meltzer MS, Nakamura M, Hansen BD, Turpin JA, Kalter DC, Gendelman HE. Macrophages as susceptible targets for HIV infection, persistent viral reservoirs in tissue, and key immunoregulatory cells that control levels of virus replication and extent of disease. AIDS Res Hum Retroviruses. 1990; 6(8):967–971. [PubMed: 2223243]

29. Meltzer MS, Skillman DR, Gomatos PJ, Kalter DC, Gendelman HE. Role of mononuclear phagocytes in the pathogenesis of human immunodeficiency virus infection. Annu Rev Immunol. 1990; 8:169–194. [PubMed: 2188662]

30. Blyth CC, Hale K, Palasanthiran P, O'Brien T, Bennett MH. Antifungal therapy in infants and children with proven, probable or suspected invasive fungal infections. Cochrane Database Syst Rev. 2010; 2:CD006343. [PubMed: 20166083]

31. Chu P, Sadullah S. The current role of amphotericin B lipid complex in managing systemic fungal infections. Curr Med Res Opin. 2009; 25(12):3011–3020. [PubMed: 19849324]

32. Pagano L, Caira M, Valentini CG, Posteraro B, Fianchi L. Current therapeutic approaches to fungal infections in immunocompromised hematological patients. Blood Rev. 2010; 24(2):51–61. [PubMed: 20056300]

33. Destache CJ, Belgum T, Christensen K, Shibata A, Sharma A, Dash A. Combination antiretroviral drugs in PLGA nanoparticle for HIV-1. BMC Infect Dis. 2009; 9:198. [PubMed: 20003214]

34. Destache CJ, Belgum T, Goede M, Shibata A, Belshan MA. Antiretroviral release from poly(DL-lactide-co-glycolide) nanoparticles in mice. J Antimicrob Chemother. 2010; 65(10):2183–2187. [PubMed: 20729545]

35. Beduneau A, Ma Z, Grotepas CB, et al. Facilitated monocyte-macrophage uptake and tissue distribution of superparmagnetic iron-oxide nanoparticles. PLoS ONE. 2009; 4(2):e4343. [PubMed: 19183814]
36. Brynskikh AM, Zhao Y, Mosley RL, et al. Macrophage delivery of therapeutic nanozymes in a murine model of Parkinson's disease. Nanomed (Lond). 2010; 5(3):379–396.
37. Gorantla S, Dou H, Boska M, et al. Quantitative magnetic resonance and SPECT imaging for macrophage tissue migration and nanoformulated drug delivery. J Leukoc Biol. 2006; 80(5):1165–1174. [PubMed: 16908517]
38. Liu Y, Uberti MG, Dou H, et al. Ingress of blood-borne macrophages across the blood–brain barrier in murine HIV-1 encephalitis. J Neuroimmunol. 2008; 200(1–2):41–52. [PubMed: 18653244]
39. Bareford LM, Swaan PW. Endocytic mechanisms for targeted drug delivery. Adv Drug Deliv Rev. 2007; 59(8):748–758. [PubMed: 17659804]
40. Bressani R, Nowacek A, Singh S, et al. Pharmacotoxicology of monocyte-macrophage nanoformulated antiretroviral drug uptake and carriage. Nanotoxicology. 2010 Epub ahead of print.
41. Marre S, Jensen KF. Synthesis of micro and nanostructures in microfluidic systems. Chem Soc Rev. 2010; 39(3):1183–1202. [PubMed: 20179831]
42. Muchow M, Maincent P, Muller RH. Lipid nanoparticles with a solid matrix (SLN, NLC, LDC) for oral drug delivery. Drug Dev Ind Pharm. 2008; 34(12):1394–1405. [PubMed: 18665980]
43▪. Takatsuka T, Endo T, Jianguo Y, Yuminoki K, Hashimoto N. Nanosizing of poorly water soluble compounds using rotation/revolution mixer. Chem Pharm Bull (Tokyo). 2009; 57(10):1061–1067. Demonstrated how poorly water soluble compounds could be prepared into nanoparticles by wet milling. In addition, they showed that the physical properties of the crystalline particles could be manipulated by altering the manufacturing process. [PubMed: 19801859]
44. Kumari S, Mg S, Mayor S. Endocytosis unplugged: multiple ways to enter the cell. Cell Res. 2010; 20(3):256–275. [PubMed: 20125123]
45. Hattula K, Furuhjelm J, Tikkanen J, Tanhuanpaa K, Laakkonen P, Peranen J. Characterization of the rab8-specific membrane traffic route linked to protrusion formation. J Cell Sci. 2006; 119(Pt 23):4866–4877. [PubMed: 17105768]
46. Junutula JR, De Maziere AM, Peden AA, et al. Rab14 is involved in membrane trafficking between the Golgi complex and endosomes. Mol Biol Cell. 2004; 15(5):2218–2229. [PubMed: 15004230]
47. Lombardi D, Soldati T, Riederer MA, Goda Y, Zerial M, Pfeffer SR. Rab9 functions in transport between late endosomes and the trans Golgi network. EMBO J. 1993; 12(2):677–682. [PubMed: 8440258]
48. Seaman MN. Endosome protein sorting: motifs and machinery. Cell Mol Life Sci. 2008; 65(18):2842–2858. [PubMed: 18726175]
49. Barbero P, Bittova L, Pfeffer SR. Visualization of Rab9-mediated vesicle transport from endosomes to the trans-Golgi in living cells. J Cell Biol. 2002; 156(3):511–518. [PubMed: 11827983]
50. Bonifacino JS, Rojas R. Retrograde transport from endosomes to the trans-Golgi network. Nat Rev Mol Cell Biol. 2006; 7(8):568–579. [PubMed: 16936697]
51. Hoekstra D, Tyteca D, van ISC. The subapical compartment: a traffic center in membrane polarity development. J Cell Sci. 2004; 117(Pt 11):2183–2192. [PubMed: 15126620]
52▪. Hsu VW, Prekeris R. Transport at the recycling endosome. Curr Opin Cell Biol. 2010; 22(4):528–534. Reviews the family of Rab proteins and discusses how they function to regulate membrane and intracellular trafficking and recycling of material. [PubMed: 20541925]
53. Jing J, Prekeris R. Polarized endocytic transport: the roles of rab11 and rab11-fips in regulating cell polarity. Histol Histopathol. 2009; 24(9):1171–1180. [PubMed: 19609864]
54. Jones MC, Caswell PT, Norman JC. Endocytic recycling pathways: emerging regulators of cell migration. Curr Opin Cell Biol. 2006; 18(5):549–557. [PubMed: 16904305]
55. Maxfield FR, McGraw TE. Endocytic recycling. Nat Rev Mol Cell Biol. 2004; 5(2):121–132. [PubMed: 15040445]

56. Sonnichsen B, De Renzis S, Nielsen E, Rietdorf J, Zerial M. Distinct membrane domains on endosomes in the recycling pathway visualized by multicolor imaging of Rab4, Rab5, and Rab11. J Cell Biol. 2000; 149(4):901–914. [PubMed: 10811830]

57. Zerial M, McBride H. Rab proteins as membrane organizers. Nat Rev Mol Cell Biol. 2001; 2(2): 107–117. [PubMed: 11252952]

58. Cayouette S, Bousquet SM, Francoeur N, et al. Involvement of Rab9 and Rab11 in the intracellular trafficking of TRPC6. Biochim Biophys Acta. 2010; 1803(7):805–812. [PubMed: 20346379]

59. Sheff DR, Daro EA, Hull M, Mellman I. The receptor recycling pathway contains two distinct populations of early endosomes with different sorting functions. J Cell Biol. 1999; 145(1):123–139. [PubMed: 10189373]

60. Ullrich O, Reinsch S, Urbe S, Zerial M, Parton RG. Rab11 regulates recycling through the pericentriolar recycling endosome. J Cell Biol. 1996; 135(4):913–924. [PubMed: 8922376]

61. van der Sluijs P, Hull M, Huber LA, Male P, Goud B, Mellman I. Reversible phosphorylation – dephosphorylation determines the localization of Rab4 during the cell cycle. EMBO J. 1992; 11(12):4379–4389. [PubMed: 1425574]

62. Chen W, Wandinger-Ness A. Expression and functional analyses of Rab8 and Rab11a in exocytic transport from trans-Golgi network. Methods Enzymol. 2001; 329:165–175. [PubMed: 11210533]

63. Larance M, Ramm G, Stockli J, et al. Characterization of the role of the Rab GTPase-activating protein as160 in insulin-regulated GLUT4 trafficking. J Biol Chem. 2005; 280(45):37803–37813. [PubMed: 16154996]

64. Cox D, Lee DJ, Dale BM, Calafat J, Greenberg S. A Rab11-containing rapidly recycling compartment in macrophages that promotes phagocytosis. Proc Natl Acad Sci USA. 2000; 97(2): 680–685. [PubMed: 10639139]

65. Jordens I, Marsman M, Kuijl C, Neefjes J. Rab proteins, connecting transport and vesicle fusion. Traffic. 2005; 6(12):1070–1077. [PubMed: 16262719]

66. Vendeville A, Rayne F, Bonhoure A, Bettache N, Montcourrier P, Beaumelle B. HIV-1 TAT enters T cells using coated pits before translocating from acidified endosomes and eliciting biological responses. Mol Biol Cell. 2004; 15(5):2347–2360. [PubMed: 15020715]

67. Murray JL, Mavrakis M, McDonald NJ, et al. Rab9 GTPase is required for replication of human immunodeficiency virus type 1, filoviruses, and measles virus. J Virol. 2005; 79(18):11742–11751. [PubMed: 16140752]

68▪. Varthakavi V, Smith RM, Martin KL, et al. The pericentriolar recycling endosome plays a key role in Vpu-mediated enhancement of HIV-1 particle release. Traffic. 2006; 7(3):298–307. Demonstrated that Vpu-mediated HIV particle release occurs via recycling endosomes. This suggests that vital parts of the HIV lifecycle occurs within recycling compartments. [PubMed: 16497224]

69. Jovic M, Sharma M, Rahajeng J, Caplan S. The early endosome: a busy sorting station for proteins at the crossroads. Histol Histopathol. 2010; 25(1):99–112. [PubMed: 19924646]

70. Yamamoto H, Koga H, Katoh Y, Takahashi S, Nakayama K, Shin HW. Functional cross-talk between Rab14 and Rab4 through a dual effector, RUFY1/Rabip4. Mol Biol Cell. 2010; 21(15): 2746–2755. [PubMed: 20534812]

71. Luzio JP, Parkinson MD, Gray SR, Bright NA. The delivery of endocytosed cargo to lysosomes. Biochem Soc Trans. 2009; 37(Pt 5):1019–1021. [PubMed: 19754443]

72. Blott EJ, Griffiths GM. Secretory lysosomes. Nat Rev Mol Cell Biol. 2002; 3(2):122–131. [PubMed: 11836514]

73. Parent A, Hamelin E, Germain P, Parent JL. Rab11 regulates the recycling of the β2-adrenergic receptor through a direct interaction. Biochem J. 2009; 418(1):163–172. [PubMed: 18983266]

74. Pasqualato S, Senic-Matuglia F, Renault L, Goud B, Salamero J, Cherfils J. The structural GDP/GTP cycle of Rab11 reveals a novel interface involved in the dynamics of recycling endosomes. J Biol Chem. 2004; 279(12):11480–11488. [PubMed: 14699104]

75. Schonteich E, Wilson GM, Burden J, et al. The Rip11/Rab11-FIP5 and kinesin II complex regulates endocytic protein recycling. J Cell Sci. 2008; 121(Pt 22):3824–3833. [PubMed: 18957512]

Websites

101. JACoP plugins http://rsb.info.nih.gov/ij/plugins/track/jacop. html 102 UniProt accession numbers www.uniprot.org 103 Subcellular localization database http://locate.imb.uq.edu.au 104 Entrez PubMed www.ncbi.nlm.nih.gov/pubmed

Executive summary

- Antiretroviral therapy (ART) has greatly reduced the morbidity and mortality associated with HIV infection; however, these drugs have limitations for both pharmacokinetics and biodistribution. This reduces their effectiveness and leads to untoward toxic side effects. Thus, the need to improve ART delivery has led to the development of nanoART.
- Packing ART into crystalline nanoformulations to facilitate monocyte-derived macrophage (MDM) cell and tissue transport could overcome the limitations associated with oral administration of free drug. The types of drug particles used in a cell-mediated delivery system are stable, efficacious and show limited or no toxicities to cells and tissues.
- Ritonavir nanoparticles (RTV-NPs) were manufactured by homogenization and then characterized. Their physical properties, rapid uptake, slow release and antiretroviral efficacy were demonstrated. By using chemical inhibitors of clathrin or caveolin we demonstrate that the drug nanoparticles enter MDM primarily by clathrin-coated pits.
- Proteomic analysis identified 38 proteins that are associated with distinct endosomal compartments. These proteins were distributed predominantly within early endosomes and recycling endosomes (RE) while fewer were located within the late endosomes or lysosomes.
- Confocal microscopy demonstrated that RTV-NP were contained predominantly within RE subcellular compartments as markers for Rab8, 11 and 14 colocalized with the particles more than others. RTV-NP was also found primarily contained within nondegradative endosomes.
- Functional disruption using siRNA and brefeldin A demonstrated that RTV-NP was primarily released by slow recycling to the plasma membrane through $Rab11^+$ endosomes. However, some particles were quickly released by fast recycling through Rab8, 14^+ endosomes.
- Immune isolation of subcellular compartments from RTV-NP loaded MDM demonstrated that the particles were contained within the endosomes in which they were identified by proteomic and confocal analysis.
- Intact particles were identified in MDM culture fluids by electron microscopy, indicating that the particles are released unmodified by cells. Released RTV-NPs were as efficacious as native drug particles at inhibiting HIV-1 replication. This demonstrated that drug particles were not morphologically altered as a result of cell-mediated transport. Together, this suggests that MDM can truly act as ‘Trojan horses’ for drug delivery to viral tissue sanctuaries.
- After RTV-NPs are taken into MDMs by clathrin-coated pits there are three pathways by which they can be trafficked back to the cell membrane for release: fast recycling via Rab8, 14^+ RE; release via secretory lysosomes; or primarily slow recycling via $Rab11^+$ RE.
- The subcellular localization of RTV-NP underlies their slow release kinetics and long-term antiretroviral efficacy. In addition, there appears to be much overlap between the subcellular trafficking of drug particles and HIV lifecycle. As such, nanoART could potentially be used to target the delivery of active drug to the

same endosomal compartments inhabited by HIV, thus greatly increasing therapeutic gains.

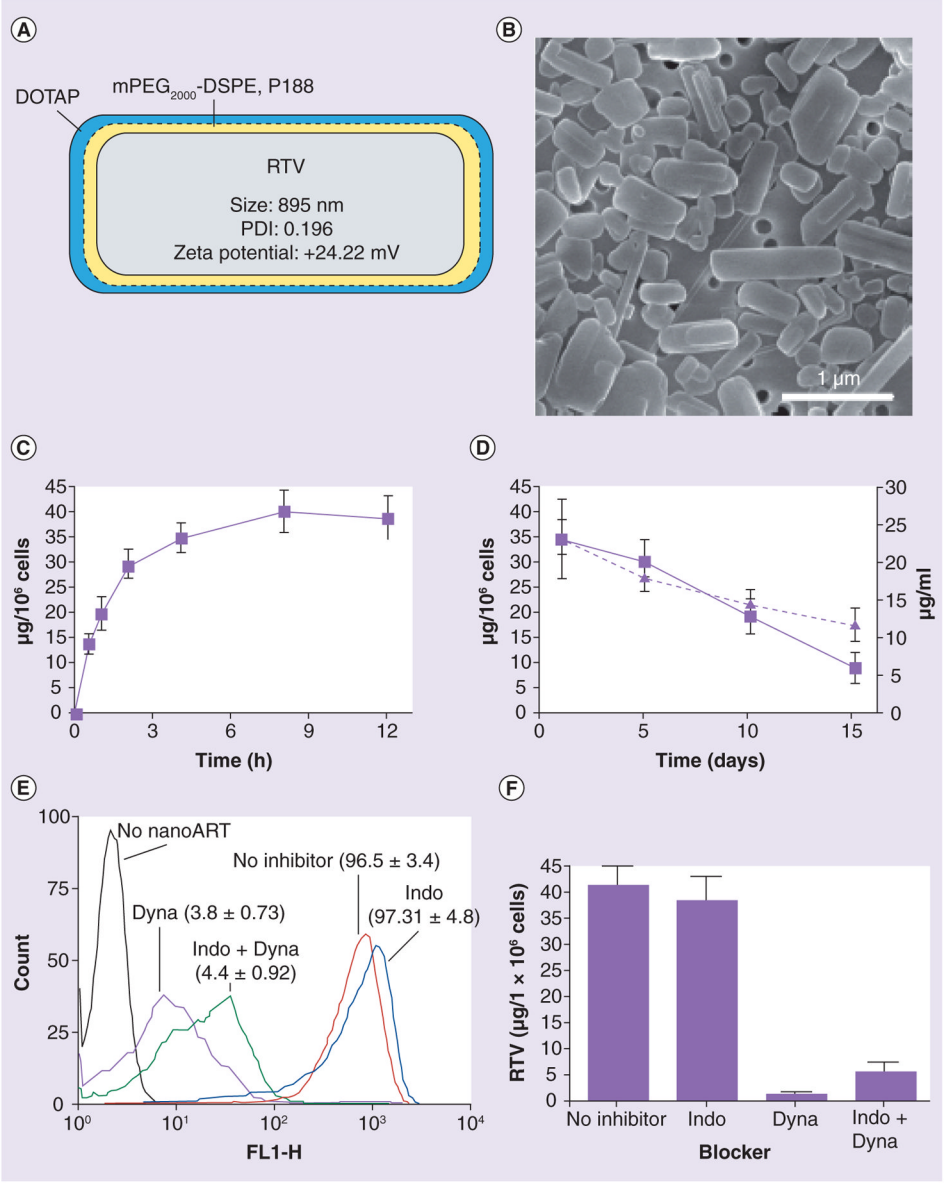

Figure 1. Characterization of the ritonavir nanoparticle and its cellular interactions

(A) RTV-NP with measurements of physical properties and depicting coating of an inner layer of $mPEG_{2000}$-DSPE/188 and an outer layer of DOTAP. Size and charge were determined by dynamic light scattering. At least four iterations for each reading were taken with <2% variance. **(B)** Scanning electron microscopy (magnification, 15,000×) of RTV-NP on top of a 0.2-µm polycarbonate membrane shows typical morphology resembling short rods with smooth edges. **(C)** Uptake of RTV-NP in monocyte-derived macrophages (MDMs) over 12 h and **(D)** retention of RTV-NP within MDMs (left y-axis) and release of drug to surrounding media (right y-axis) over 15 days were determined by high-performance liquid chromatography. **(E)** Flow cytometry data and **(F)** high-performance liquid chromatography data of MDMs exposed to fluorescent RTV-NPs demonstrate that treating MDMs with the clathrin inhibitor Dyna significantly reduces uptake. All data represent the mean ± standard error of the mean for n = 3.

ART: Antiretroviral therapy; DOTAP: Dioleoyl trimethylammonium propane; Dyna: Dynasore; Indo: Indomethacin; NP: Nanoparticle; RTV: Ritovanir.

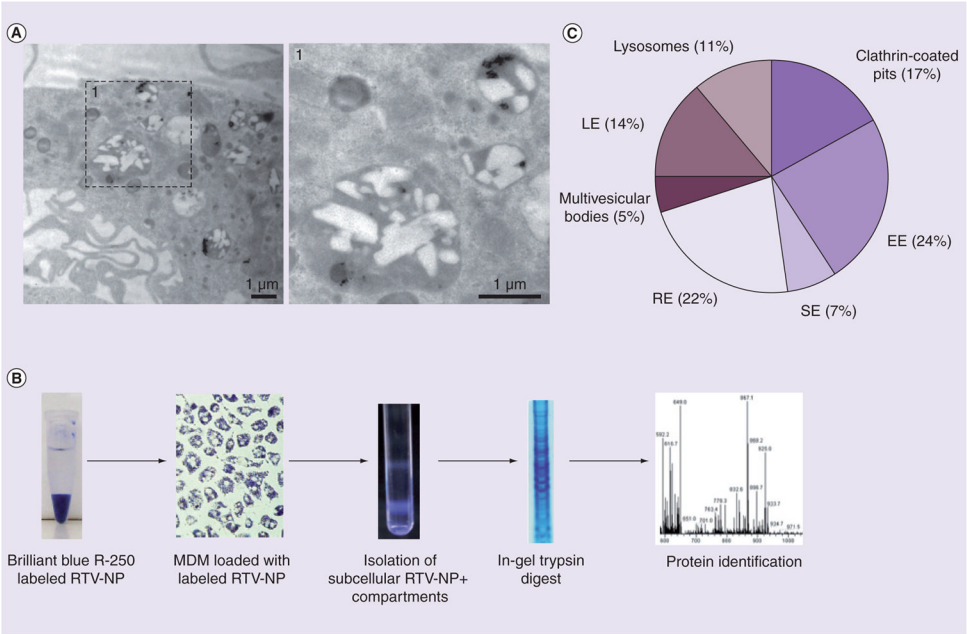

Figure 2. Proteomic analyses of RTV-NP locale

(A) Intracellular RTV-NP were identified within distinct membrane-bound compartments by transmission electron microscopy (magnification 15,000×). **(B)** The subcellular localization process. RTV-NP were labeled with Brilliant Blue-250 and exposed to MDM. The cells were lysed and subcellular compartments separated by centrifugation on a sucrose gradient. Blue bands represent compartments that contain RTV-NP. These bands were collected, and the proteins separated by electrophoresis. Following in-gel trypsin digest, the proteins were identified using liquid chromatography/mass spectrometry. **(C)** Subcellular distribution of the identified proteins. A total of 38 endosomal proteins were identified. Each protein was included in each category in which it was identified up to this point in time. Proteomic analysis indicated that RTV-NP distribution was primarily with RE and EE compartments. EE: Early endosomes; LE: Late endosomes; MDM: Monocyte-derived macrophage; NP: Nanoparticle; RE: Recycling endosomes; RTV: Ritovanir; SE: Sorting endosomes.

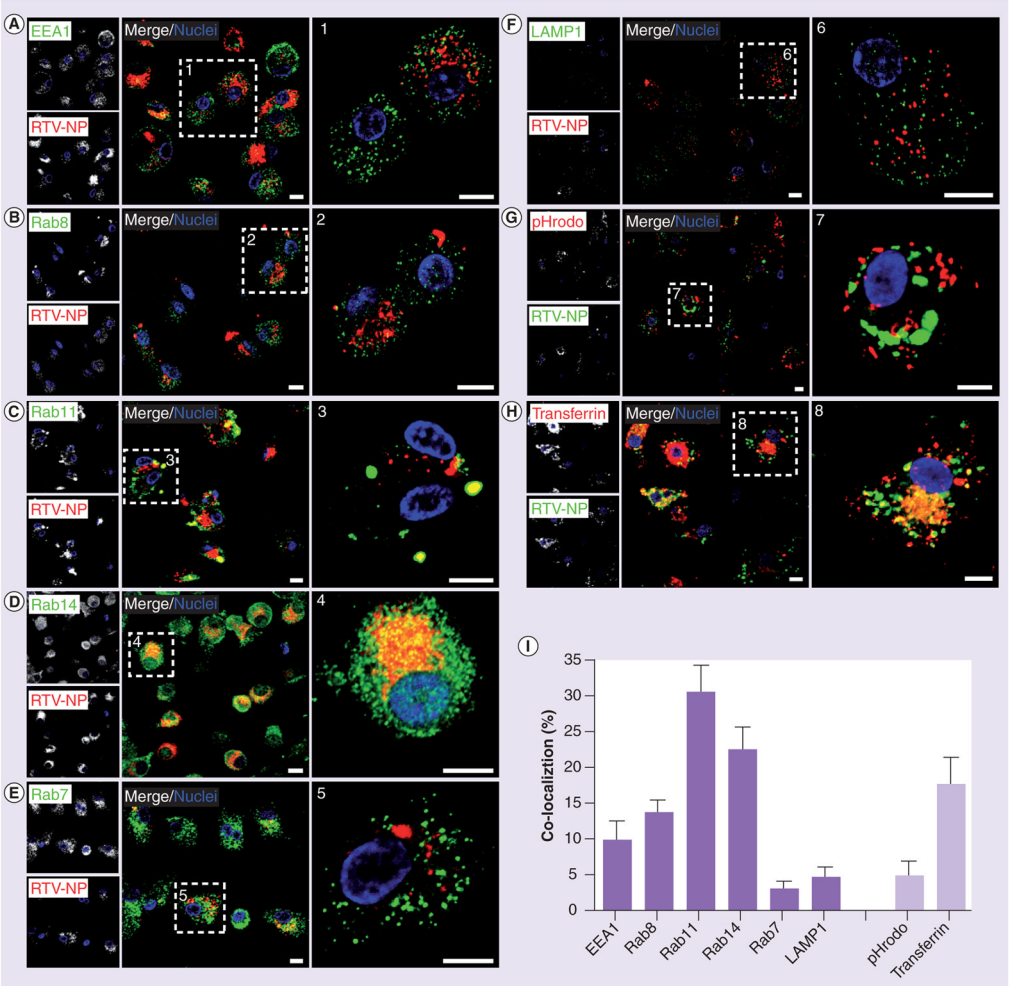

Figure 3. Immunohistological identification of nanoparticle subcellular localization

(A–H) Confocal microscopy confirmed distribution of RTV-NP within endocytic compartments. Note that RTV-NP are **(A–F)** red and **(G–H)** green, and yellow signifies marker-particle overlap in all panels. **(I)** Pearson's colocalization coefficients indicate RTV-NPs are preferentially distributed to Rab11 and Rab14 recycling endosomes compared with early endosomes, Rab8 or Rab7 endosomes, and lysosomes. Analysis of distribution of RTV-NP within acidified (degrading) compartments, identified by pHrodo-dextran beads, revealed minimal overlap indicating RTV-NP likely bypass degradation within the cell and are primarily recycled for release. High RTV-NP colocalization with transferrin also indicates that particles are most likely recycled. Measure bars equal 1 μm. Graphical data represent the mean ± standard error of the mean for n = 3. NP: Nanoparticle; RTV: Ritonavir.

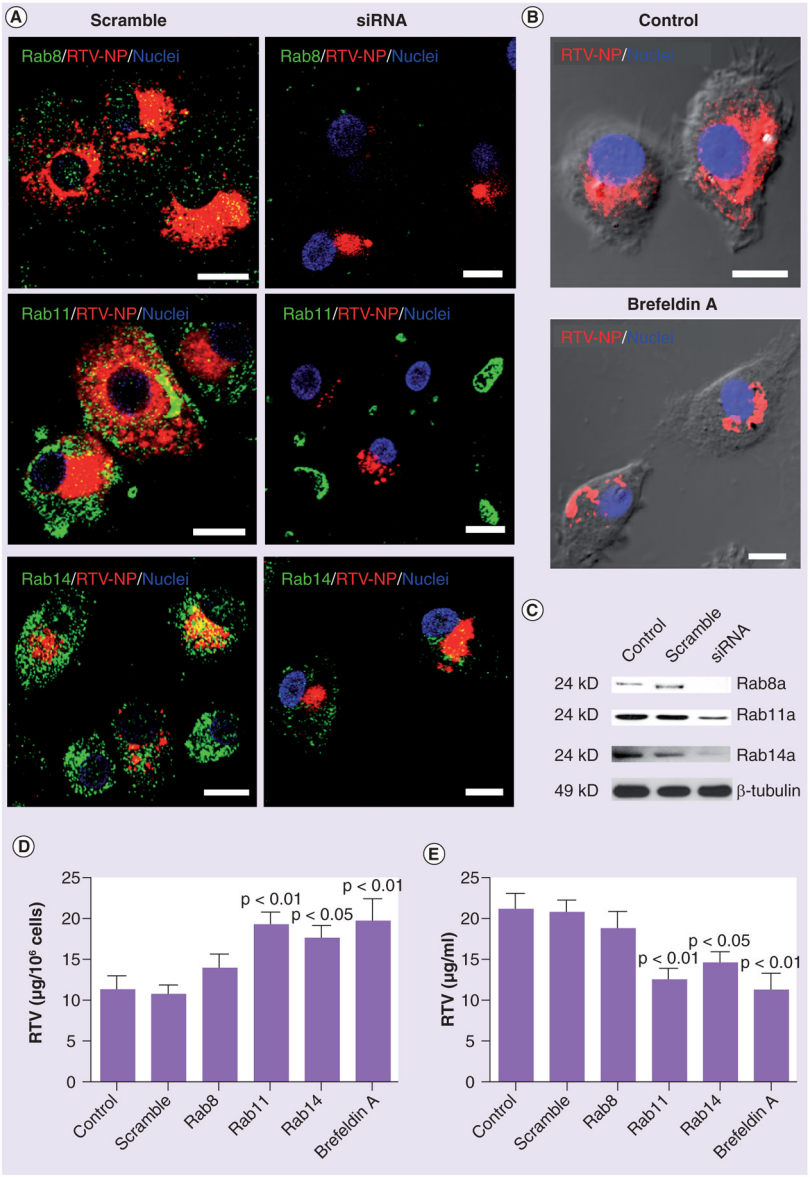

Figure 4. Validation of nanoparticle subcellular localization

(A & B) Disruption of endocytic recycling with siRNA (Rab8, 11 and 14) as well as disruption of cell secretion with brefeldin A resulted in knockout of the associated protein and caused RTV-NPs to be redistributed within monocyte-derived macrophages. **(A & B)** In each case, siRNA treatment resulted in aggregation of RTV-NPs at the perinuclear region within large vacuoles. **(C)** siRNA silencing of specific proteins was confirmed by Western blot. High-performance liquid chromatography quantitation of RTV-NP in **(D)** cells and **(E)** culture fluids demonstrated that disruption of endocytic recycling and inhibition of secretion significantly increased cellular retention of RTV-NPs and reduced release. Upper p-value signifies difference from control cells and lower p-value signifies difference from cells treated with scrambled siRNA. Measure bars equal 1 μm. Graphical data represent the mean ± standard error of the mean for n = 3.

NP: Nanoparticle; RTV: Ritonavir.

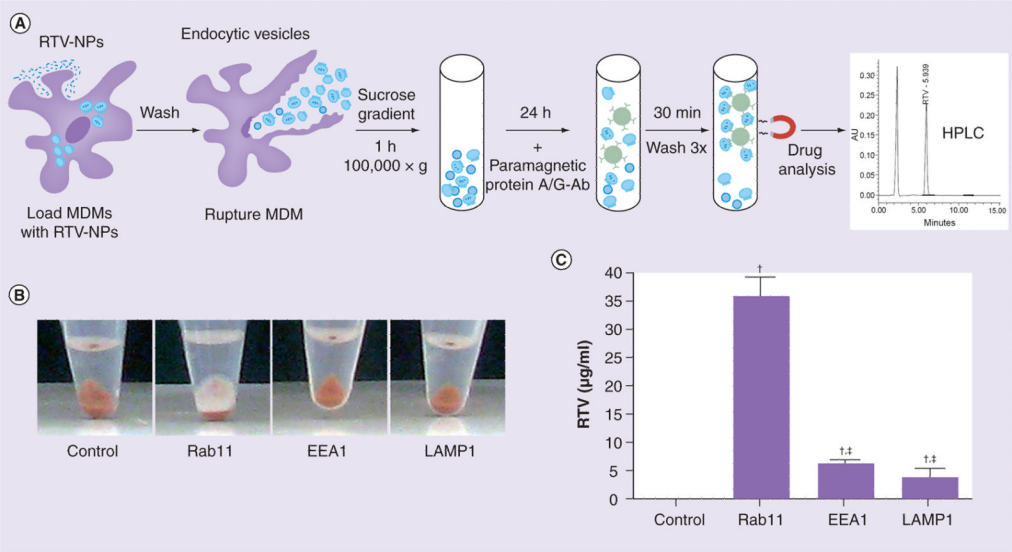

Figure 5. Ritonavir nanoparticles are transported during endocytic sorting

Since RTV-NPs were labeled with lipophillic dyes (DiD or DiO), which bind to the polymer coat but not the drug crystal itself, we tested whether the endocytic distribution of drug matched that of labeled polymer. **(A)** Treatment of MDM with RTV-NP and subsequent immune isolation of subcellular compartments and HPLC analysis of drug content. **(B)** Image of magnetic beads along with immune isolated endosomal compartments prior to HPLC analysis; the white matter on top of the bead pellet in the Rab11 tube was presumably RTV-NP filled endosomes. **(C)** HPLC analyses of immune isolated compartments confirmed a greater amount of RTV present in Rab11 endosomes than in either EEA1 or LAMP1. Graphical data represent the mean ± standard error of the mean for n = 3.

†Significantly ($p < 0.01$) different from control.

‡Significantly ($p < 0.01$) different from Rab11.

Ab: Antibody; HPLC: High-performance liquid chromatography; MDM: Monocyte-derived macrophage; NP: Nanoparticle; RTV: Ritovanir.

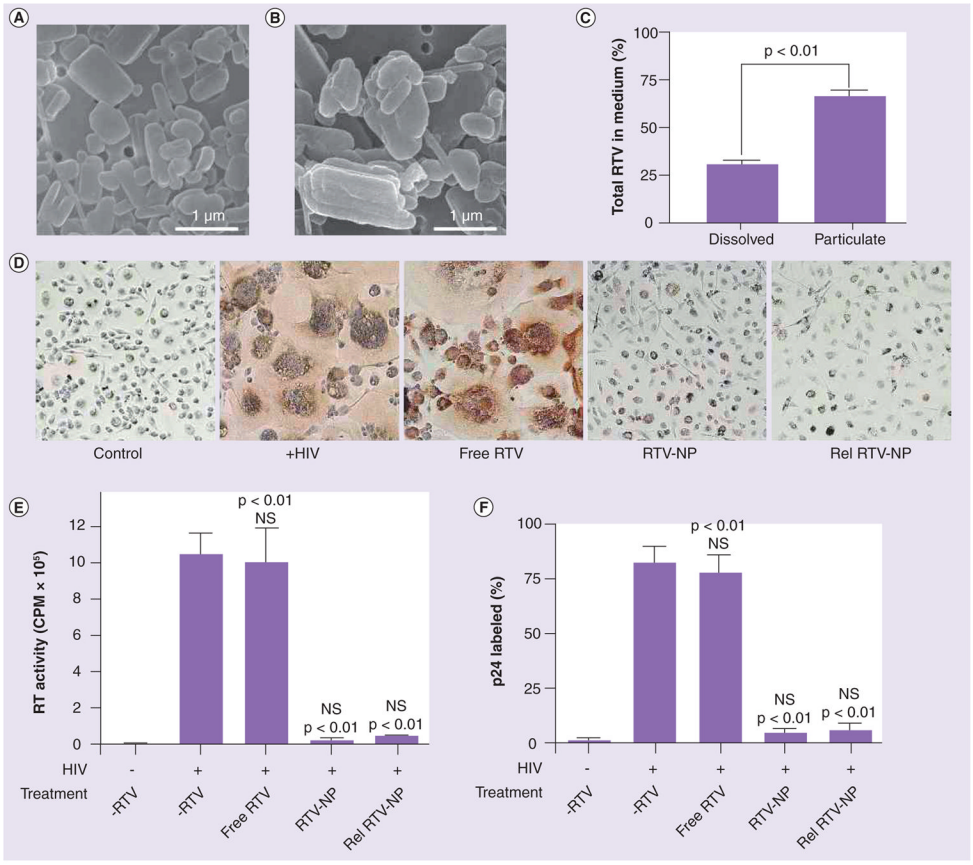

Figure 6. Ritovanir nanoparticles are released intact and retain their antiretroviral efficacy

The data indicated that RTV-NPs were not being degraded but were recycled through the cell, suggesting that intact RTV-NPs should be released. Scanning electron microscopy (magnification 15,000×) of native RTV-NPs **(A)** and RTV-NPs released from cells into the surrounding medium **(B)**. RTV-NPs were separated from dissolved drug by ultracentrifugation; the percentage of total drug in both particulate and dissolved form is shown. Total drug concentration was 40 µg/ml **(C)**. Monocyte-derived macrophages were treated with either free RTV, native RTV-NP or released RTV-NP and subsequently challenged with HIV. Treatment of monocyte-derived macrophages with released RTV-NP reduced viral infection to similar levels as the native (non-endocytosed) particles as seen by p24 staining and formation of multinucleated giant cells **(D)**, measurement of RT activity **(E)**, and density of p24 staining **(F)**. For both RT activity and p24 density measurements all data represent the mean ± standard error of the mean for n = 4.

NP: Nanoparticle; NS: Nonsignificant; RT: Retroviral; RTV: Ritovanir.

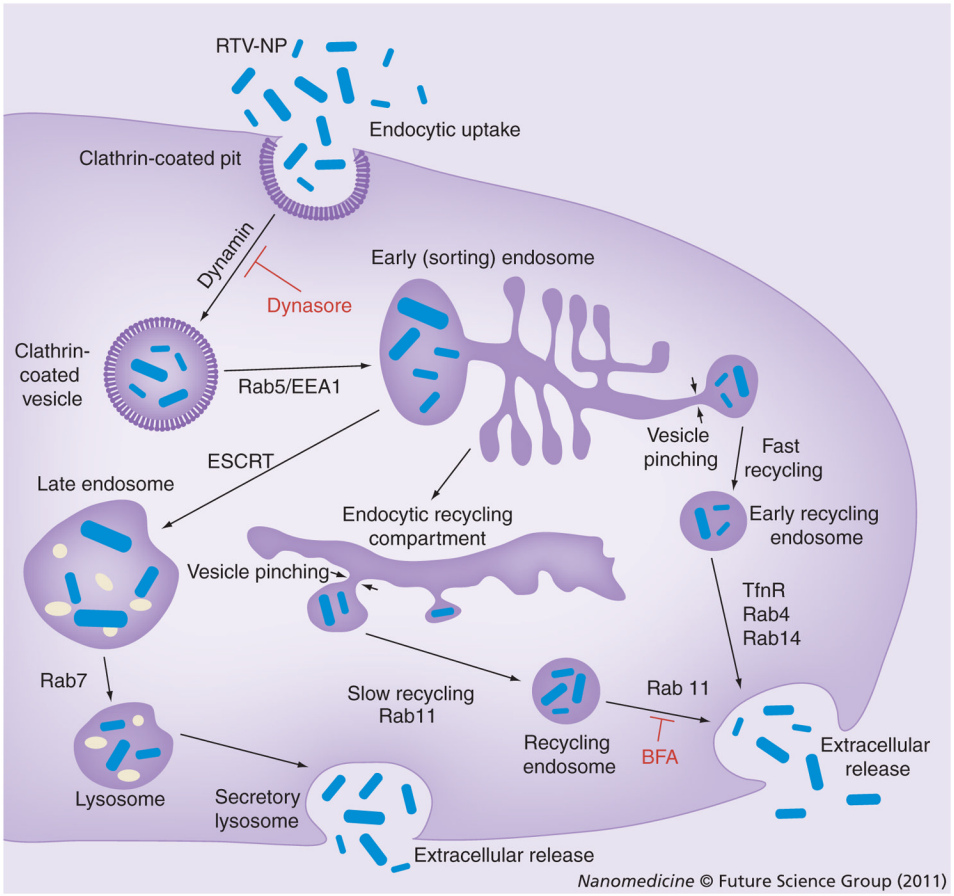

Figure 7. Intracellular pathways of ritonavir nanoparticles

RTV-NPs (shown in blue) enter MDM via clathrin-coated pits and are then transported to the early endosome (EE) compartment. From the EE compartment, the particles can have three different fates: fast recycling via Rab4^{+} or 14^{+} endosomes [69,70]; trafficking to late endosome, regulated in part by ESCRT machinery [71] for eventual release as a secretory lysosome [72]; or for most of the particles, transport to the recycling endosome (RE) compartment where they will be stored for long periods and slowly recycled via Rab11^{+} endosomes [73–75].

BFA: Brefeldin A; ESCRT: Endosomal sorting complex required for transport; NP: Nanoparticle; RTV: Ritonavir.

Table 1

Protein markers associated with ritonavir-nanoparticle-containing endosomes.

Protein ID	Peptide No[†]	MW (Da)[‡]	UniProt No[§]	Vesicle compartment[¶]	Function[#]
Annexin I	8	38,714	P04083	EE, MVB	Endocytosis and exocytosis
Annexin A2	12	38,604	P07355	CCP, EE, SE, MVB, RE, LE	Endocytosis and exocytosis
Annexin IV	7	36,085	P09525	EE, SE, RE	Endocytosis and exocytosis
Pro-low-density lipoprotein receptor-related protein 1	5	504,578	Q07954	CCP	Endocytosis and exocytosis
Ezrin	2	69,398	P15311	CCP, EE, RE, L	Endocytosis and exocytosis
Myosin-9	17	226,530	P35579	EE, RE	Endocytic transport
Myosin light polypeptide 6	3	16,961	Q60605	RE	Endocytic transport
Tropomyosin-4	3	28,522	P67936	RE	Endocytic transport
Rho GDP dissociation inhibitor 2	2	22,988	P52566	EE, SE, RE	Endocytic transport
Early endosome antigen 1	4	162,466	Q15075	EE, SE	Endocytic trafficking
Rab5C	2	23,482	P51148	CCP, EE, SE, RE	Endocytic trafficking
Rab7A	2	23,490	P51149	LE, L	Endocytic trafficking
Rab8B	3	23,584	Q92930	CCP, SE, RE	Endocytic trafficking
Rab9B	3	22,719	Q9NP90	RE, LE	Endocytic trafficking
Rab11B	5	24,573	Q15907	RE	Endocytic trafficking
Rab14	4	23,927	P61106	CCP, EE, RE	Endocytic trafficking
Syntaxin-7	2	29,815	O15400	CCP, EE, RE, LE, L	Endocytic trafficking
α-actinin-4	3	102,268	O43707	CCP, EE, SE, RE, LE, L	Endocytic trafficking
Clathrin heavy chain 1	7	191,613	Q00610	CCP, EE, RE	Endocytic trafficking
Glyceraldehyde-3-phosphate dehydrogenase	2	36,053	P04406	CCP, EE, RE	Endocytic trafficking
Myoferlin	7	234,706	Q9NZM1	CCP, EE, RE	Endocytic trafficking
Platelet endothelial cell adhesion molecule	4	82,536	P16284	EE, LE	Endocytic trafficking
Lysosome-associated membrane glycoprotein 1	3	44,882	P11279	LE, L	Endocytic trafficking
α-actin-1	3	42,051	P68133	CCP	Cell migration
Annexin VI	8	75,873	P08133	CCP, EE, RE, MVB	Ion transport
Na^+/K^+-ATPase α 1 subunit	5	112,895	P05023	CCP, EE, RE	Ion transport

Protein ID	Peptide No†	MW (Da)‡	UniProt No§	Vesicle compartment¶	Function#
Na^+/K^+-ATPase α 2 subunit	2	112,265	P50993	CCP, EE, RE	Ion transport
Annexin A5	8	35,936	P08758	EE, LE	Signal transduction
Lymphocyte activation antigen 4F2 large subunit (CD98)	8	57,945	P08195	EE, RE	Amino acid transport
HLA class I histocompatibility antigen, B-52 α chain	2	40,521	P30490	RE, MVB	Immune response
Synaptic vesicle membrane protein VAT-1 homolog	4	41,920	Q99536	CCP, EE, LE, L	Redox
Peroxiredoxin-1	3	22,110	Q06830	EE, SE, RE, LE, L	Redox
Retinol dehydrogenase 11	3	35,386	Q8TC12	LE, L	Redox
Heat-shock protein HSP 90-β	5	83,264	P08238	EE, RE, LE, L	Protein folding
Heat-shock 70 kDa protein 1-like	3	70,405	P34931	CCP, EE, LE, L	Protein folding
Heat-shock cognate 71 kDa protein	5	53,517	P11142	CCP, EE, LE, L	Protein folding
Heat-shock protein HSP 90-α	2	35,760	P07900	EE, RE, LE, L	Protein folding
Protein disulfide-isomerase A3	9	56,796	P30101	MVB	Protein folding

†Number of unique significant ($p < 0.05$) peptides identified for each protein.

‡Theoretical molecular mass for the primary translation product calculated from DNA sequences.

§Accession numbers for UniProt (accessible at [102]).

¶Postulated subcellular localizations (accessible at [102,103] and literature search using [104]).

#Postulated cellular function (accessible at [102,103] and literature search using [104]).

CCP: Clathrin-coated pits; EE: Early endosomes; L: Lysosomes; LE: Late endosomes; MVB: Multivesicular bodies; RE: Recycling endosomes; SE: Sorting endosomes.